Crust–mantle mixing and crustal reworking of southern Tibet during Indian continental subduction: Evidence from Miocene high-silica potassic rocks in Central Lhasa block

Article *in* Lithos · June 2019

DOI: 10.1016/j.lithos.2019.05.035

CITATIONS
0

READS
375

6 authors, including:

Hao Lulu
University of Science and Technology of China
12 PUBLICATIONS **135** CITATIONS
SEE PROFILE

Qiang Wang
Chinese Academy of Sciences
672 PUBLICATIONS **18,391** CITATIONS
SEE PROFILE

Jin-Hui Yang
Institute of Geology and Geophysics, Chinese Academy of Sciences, Beijing, China
177 PUBLICATIONS **13,460** CITATIONS
SEE PROFILE

Lin Ma
Chinese Academy of Sciences
31 PUBLICATIONS **492** CITATIONS
SEE PROFILE

Lithos 342–343 (2019) 407–419

Contents lists available at ScienceDirect

Lithos

journal homepage: www.elsevier.com/locate/lithos

Crust-mantle mixing and crustal reworking of southern Tibet during Indian continental subduction: Evidence from Miocene high-silica potassic rocks in Central Lhasa block

Lu-Lu Hao [a,b], Qiang Wang [a,c,d,*], Derek A. Wyman [e], Jin-Hui Yang [f], Fang Huang [b], Lin Ma [a]

[a] State Key Laboratory of Isotope Geochemistry, Guangzhou Institute of Geochemistry, Chinese Academy of Sciences, Guangzhou 510640, China
[b] CAS Key Laboratory of Crust-Mantle Materials and Environments, School of Earth and Space Sciences, University of Science and Technology of China, Hefei 230026, China
[c] CAS Center for Excellence in Tibetan Plateau Earth Sciences, Beijing 100101, China
[d] College of Earth and Planetary Sciences, University of Chinese Academy of Sciences, Beijing 10049, China
[e] School of Geosciences, The University of Sydney, NSW 2006, Australia
[f] Institute of Geology and Geophysics, Chinese Academy of Science, Beijing 100029, China

ARTICLE INFO

Article history:
Received 20 February 2019
Revised 25 May 2019
Accepted 29 May 2019
Available online 01 June 2019

ABSTRACT

Collisional zones are commonly considered as important regions for crustal reworking, but the reworking mechanism remains debated. The well-known Himalayan-southern Tibetan orogen, built by India-Asia collision and convergence, has the thickest continental crust on Earth and is therefore an ideal region for studying crustal reworking during collisional orogenesis. Here we revisit the Miocene high-silica potassic rocks (trachytes) in the Konglong area of the central Lhasa block, southern Tibet. Integrated studies of geochronology, mineral compositions, bulk-rock major- and trace-element geochemistry, and Sr-Nd-Pb-Hf-O isotopes unequivocally indicate that the Konglong trachytes formed by mixing between enriched mantle-derived ultrapotassic and thickened ancient crust-derived magmas. Combined with post-collisional magma mixing recently identified in the southern Lhasa block, we suggest that magma underplating and subsequent mantle-crust interaction (i.e., the matter and energy transfer from the mantle to the crust) has been a common and important crustal reworking process in southern Tibet during Indian continental subduction. This process may be related to Indian plate flat subduction and subsequent foundering during the post-collisional stage. In combination with the nature of Cenozoic magmatism in the Himalaya block, we suggest that in addition to partial melting of the subducted continental crust, magma underplating and subsequent crust-mantle mixing beneath the obducted continent has also played an important role in crustal reworking of the collisional zone.

1. Introduction

Earth's convergent plate margins (oceanic subduction and continental collision zones) are important locations for continental crustal evolution (growth and reworking) (Castro et al., 2013; Ernst, 2010; Hao et al., 2016a; Hawkesworth et al., 2016; Kelemen, 1995; Rudnick, 1995; Sengör et al., 1993; Zheng et al., 2007, 2008, 2015). Specifically, oceanic subduction zones may be the most important regions for continental crustal growth (Chen and Arakawa, 2005; Jahn, 2004; Rudnick, 1995). For instance, the combination of vertical addition of juvenile basaltic components from oceanic subduction-related magmatism into island arc crust (Rudnick, 1995) and subsequent lateral accretion of the island arc to a continental plate (Sengör et al., 1993) constitutes a remarkably efficient continental crustal growth mechanism. Subduction-related continental arc magmatism commonly contributes juvenile andesitic components to continental crustal growth (Castro et al., 2010, 2013; Chen et al., 2014; Hao et al., 2016b; Taylor and McLennan, 1985). In contrast, continental collision zones were generally considered to be key regions for continental crustal reworking (Ernst, 2010; Zheng, 2012). Continental subduction zones (e.g., continent-continent or continent-arc collision) often induce partial melting of the subducted accretionary complex during the *syn*-collisional stage (Collins and Richards, 2008; Zheng et al., 2011). They also generally cause syn-exhumation partial melting of the continental crust, or partial melting of the subducted continental crust retained in a continental subduction channel, to produce post-collisional granitoids (Dai et al., 2017; Gao et al., 2018; Zhao et al., 2004, 2007, 2011, 2017). For example, the Shidao late Triassic alkaline complex in the Jiaodong Peninsula of the Dabie-Sulu orogenic belt (Yang et al., 2005; Zhao et al., 2012), is widely considered to have been derived by syn-exhumation partial melting of the South China

* Corresponding author at: State Key Laboratory of Isotope Geochemistry, Guangzhou Institute of Geochemistry, Chinese Academy of Sciences, Guangzhou 510640, China.
E-mail address: wqiang@gig.ac.cn (Q. Wang).

https://doi.org/10.1016/j.lithos.2019.05.035
0024-4937/

block continental plate. Similarly, the widespread early Cretaceous post-collisional granitoids of the Dabie orogen are commonly interpreted to have originated via recycling of the subducted South China block continental crust (Zhao et al., 2017).

The Himalayan-southern Tibetan orogen, as one of the most prominent Cenozoic continent-continent collision zones (Yin and Harrison, 2000), resulted from Neo-Tethyan oceanic subduction, India-Asia collision and Indian continental subduction (Chung et al., 2005; DeCelles et al., 2002, 2011; Zhu et al., 2011, 2018), and is an ideal place to study crustal evolution at a convergent plate margin. Numerous studies have collectively revealed details of crustal growth in southern Tibet during Neo-Tethyan oceanic subduction by mantle- or oceanic slab-derived magma accretion (Chu et al., 2006; Ma et al., 2013a, 2013b; Mo et al., 2008; Zhang et al., 2010; Zhu et al., 2011). However, crustal reworking in the orogen during Indian continental subduction has received much less attention and has mainly been studied in the Himalaya block (Gao et al., 2017; Hou et al., 2012; Zeng et al., 2011; Zhang et al., 2004). The two episodes of granitoid magmatism in the Himalaya block is widely suggested to have been generated by partial melting of the subducted Indian continental crust during *syn*-exhumation and post-collisional crustal thinning, respectively (Hou et al., 2012; Wu et al., 2015; Zeng et al., 2011; Zhang et al., 2004). Recently, the post-collisional crustal reworking (metamorphism, anatexis and magmatism) of the southern Lhasa block (SLB) induced by Indian continental subduction and ongoing convergence was proposed (Zhang et al., 2015; Zheng and Wu, 2018). Moreover, based on their study of meta-granitoid xenoliths in the Sangsang ultrapotassic lavas, Wang et al. (2016) argued that underplating of mantle-derived ultrapotassic magmas and subsequent mantle-crust mixing was an effective mechanism for SLB crustal reworking. The ultrapotassic magmas interacted with deep crust to form hybridized granitoids, leaving a refractory residue that then underwent complex metamorphism, which was entrained as xenoliths by later ultrapotassic magmas. Indeed, post-collisional magmatic rocks generated by mixing of ultrapotassic and juvenile crust-derived adakitic magmas have increasingly been identified in the SLB (Sun et al., 2018; Yang et al., 2015), indicating that matter and energy transfer from the mantle to the crust may have played a key role in crustal reworking of southern Tibet.

As discussed above, the mechanism for crustal reworking in a collisional zone remains debated. In addition to partial melting of the subducted continental crust, mixing between mantle- and crust-derived magmas beneath the obducted continent is also likely an effective mechanism for continental crustal reworking in a collisional zone (e.g., the Himalayan-southern Tibetan orogen). However, the latter scenario requires further validation. For example, the Indian continent has subducted beneath the central Lhasa block (CLB) as revealed by geophysical data (Nabělek et al., 2009), but the question of whether magma mixing occurred in the CLB remains unclear.

A few post-collisional potassic lavas in the CLB (e.g., the Miocene trachytes in the Bugasi area) were previously suggested to be likely produced by mixing between ultrapotassic and lower crust-derived magmas (Chen et al., 2012). However, this genetic model has been hotly debated, because: (1) the post-collisional potassic (MgO < 3 wt%, not ultrapotassic) lavas in the Lhasa block, were generally considered to have been produced by other mechanisms including partial melting of crustal components (e.g., the Xungba rocks, Liu et al., 2014), and crustal assimilation and fractional crystallization processes (AFC) of ultrapotassic magmas (e.g., the Yangying rocks, Zhang et al., 2017); (2) the mixed crustal end-member for the Bugasi trachytes represented by the Konglong trachytes remains debated. Chen et al. (2010) suggested that due to absence of ultrapotassic components in the Konglong area, the Konglong trachytes are unlikely to form via AFC of ultrapotassic magmas or by magma mixing and thus should have a crustal origin. Recently, however, we identified abundant mafic igneous enclaves within the Konglong trachytes and interpreted these enclaves to have crystalized from primitive ultrapotassic magmas (Hao et al., 2018). Thus, the petrogenesis of the Konglong trachytes needs to be further investigated, and the role of magma mixing in the formation of the CLB potassic rocks has still not been fully resolved.

In this study, we revisit the Konglong Miocene trachytes (Fig. 1) and suggest that mixing between mantle-derived ultrapotassic and ancient crust-derived magmas is likely responsible for their generation, based on integrated studies of geochronology, mineral compositions, whole-rock major- and trace-element geochemistry, and Sr-Nd-Pb-Hf-O isotopes. We suggest that this newly identified magma mixing in the CLB has important implications for the crustal reworking of southern Tibet.

2. Geologic setting and samples

The Himalayan-Tibetan orogen is composed of the Himalaya, Lhasa, Qiangtang, and Songpan-Ganze blocks, from south to north, separated from each other by the Indus-Yarlung-Zangbu, Bangong-Nujiang, and Jinsha suture zones (Fig. 1). The Lhasa block of southern Tibet was the last geological terrane accreted to Eurasia in the early Cretaceous before its collision with the northward drifting Indian continent in the early Cenozoic (Yin and Harrison, 2000). During these two collage-forming processes (Lhasa-Eurasia and India-Lhasa), the Lhasa block underwent episodes of oceanic subduction (Bangong-Nujiang ocean to the north and Indus-Yarlung-Zangbu Neo-Tethyan ocean to the south), which caused significant additions of juvenile materials (i.e., magmas derived from the depleted mantle and oceanic slab) into its northern and southern edges (Zhu et al., 2013). Accordingly, the Lhasa block can be subdivided into the northern, central, and southern Lhasa subterranes, which are separated by the Shiquanhe-Nam Tso mélange zone and Luobadui-Milashan fault from north to south (Fig. 1) (Zhu et al., 2018).

The initial India-Eurasia (India-Lhasa) collision is generally suggested to have occurred in the early Cenozoic (65–55 Ma) (Hu et al., 2015). The ongoing collision, where Indian continental lithosphere is dragged by subducted Neo-Tethyan oceanic lithosphere, would induce slab breakoff (i.e., separation of the oceanic and continental lithosphere) due to the buoyancy of Indian continental lithosphere (Zhu et al., 2015). Slab breakoff most likely occurred at 50–45 Ma, based on the presence of a magmatic flare-up and OIB-type rocks (DeCelles et al., 2011; Ji et al., 2016; Jiang et al., 2014; Zhu et al., 2015). During the period from initial collision to oceanic slab breakoff, the well-known Linzizong volcanic succession (LVS) and its coeval granitoid batholiths formed (Ji et al., 2009). Oceanic slab breakoff resulted in rapid exhumation of slices of the subducted Indian continental slab, which produced the 44–35 Ma adakites and leucogranites in the Himalaya block (Hou et al., 2012).

After oceanic slab breakoff, the collision zone converted into a post-collisional intra-continent setting with Indian continental subduction beneath the Lhasa block. The widespread post-collisional magmatism in the Himalaya block is mainly composed of the 26–7 Ma leucogranites. The post-collisional magmatism is widespread in the Lhasa block and primarily consists of the 25–8 Ma isotopically-enriched ultrapotassic-potassic lavas and 26–10 Ma isotopically-depleted adakitic rocks, which are mainly distributed in the CLB and SLB, respectively (Chung et al., 2005) (Fig. 1).

Our studied post-collisional magmatism is found near the Pozico (a lake) in the Konglong area and within the south-western part of the north-south-trending TangroYumco-Xuruco graben in the central Lhasa block. The Konglong post-collisional volcanic rocks were erupted upon the Dianzhong and Nianbo Formations of the Linzizong volcanic succession and consist of two circular domes with a total area of ~ 81 km^2. Recent studies have shown that the Konglong volcanic rocks are mainly composed of trachytes with minor rhyolites (Chen et al., 2010) and A-type felsic lavas (Hao et al., 2019). Chen et al. (2010) reported a whole-rock ^{40}Ar—^{39}Ar age of ~21 Ma for a rhyolite. Our recent work (Hao et al., 2019) showed that the A-type felsic lavas with ages of 24–23 Ma could be erupted slightly earlier than the trachytes (~21 Ma) and rhyolites. We have also identified numerous mafic igneous enclaves in the Konglong trachytes, which are interpreted to have crystallized

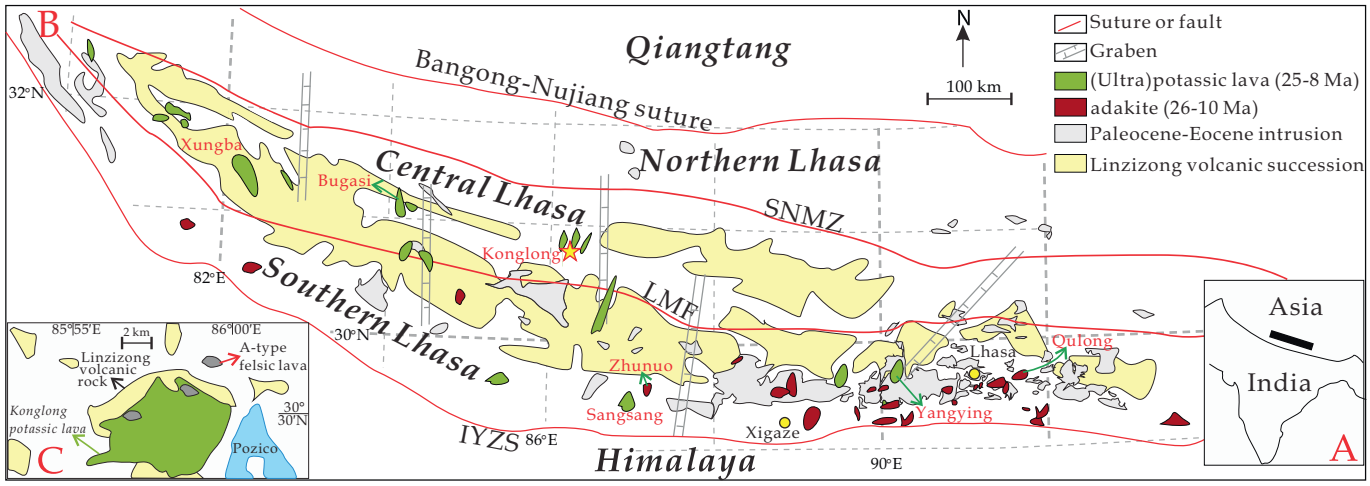

Fig. 1. (A) A sketch showing location of Tibet in regional context. (B) Geological map of southern Tibet (the Lhasa block) showing the main tectonic units and Cenozoic magmatism, modified from Wang et al. (2018). SNMZ = ShiquanRiver-NamTso Mélange Zone; LMF = Luobadui-Milashan Fault; IYZS = Indus-Yarlung-Zangbu suture. (C) Simplified map showing volcanism in the Konglong area, modified from Hao et al. (2019).

from primitive ultrapotassic magmas (Hao et al., 2018). Here, we focused on the trachytes. Representative field relationship photos and photomicrographs for the Konglong trachytes are shown in Hao et al. (2018, 2019). The trachytes are light-gray in color and show massive structure and typical porphyritic texture, with abundant phenocrysts (5–30%) in a fine trachytic groundmass. The trachytes have abundant mafic minerals [e.g., clinopyroxene (Cpx), amphibole (Amp), phlogopite (Phl)] and K-feldspar (Kfs) with minor plagioclase (Pl) and quartz (Qz) as phenocrysts (Chen et al., 2010; Hao et al., 2019). The Kfs commonly shows simple twins and is aligned and the Amp and Phl commonly have dark margins. The accessory minerals are mainly Fe—Ti oxides, apatite, and zircon. The trachytic groundmass is composed of Kfs, biotite, opaque minerals and glass.

Here, integrated studies of geochronology, mineral compositions, whole-rock major-, trace-element geochemistry, and Sr-Nd-Pb-Hf-O isotopes are used to explore the genesis of the Konglong trachytes.

3. Results

The bulk-rock and mineral geochemical and zircon U—Pb dating analytical methods have been described in Hao et al. (2018, 2019). Zircon Hf isotope measurements were done using LA-ICPMS with a beam size of 60 μm and laser pulse frequency of 8 Hz. The analytical procedures were described in detail in Wu et al. (2006). Present $^{176}Hf/^{177}Hf$ ratios for the zircon standards MUD (0.282504 ± 2) and GJ-1 (0.282018 ± 4) were in good agreement within errors with the reported values (e.g., Wu et al., 2006). The bulk-rock major, trace elemental and Sr-Nd-Pb isotopic data are showed in Table 1 and other analytical results are reported in the Supplementary Information.

3.1. Zircon U—Pb ages and Hf—O isotopes

SIMS zircon U—Pb dating of the Konglong trachyte sample (KL21−1) gives a weighted mean $^{206}Pb/^{238}U$ age of 21.3 ± 0.4 Ma (MSWD = 0.6) (Fig. 2a). Combined with previous zircon age data of the Konglong trachytes (Hao et al., 2018, 2019), we suggest that the Konglong trachytes were erupted in the early Miocene (~21 Ma), coeval with the Konglong rhyolites (Chen et al., 2010).

The Konglong trachyte samples KL02–3 and KL17–1 show similar enriched zircon εHf(t) values of −12.1 to −8.3 and − 12.6 to −8.7, respectively, comparable to those of the ultrapotassic lavas and Xungba potassic rocks (Fig. 2b). The zircons $\delta^{18}O$ data of the three samples (KL17–1, 21–1, 02–3) show similar ranges of 8.1–8.9, 8.2–8.9, 8.1–9.1 with average values of 8.46, 8.58 and 8.64, respectively (Hao et al., 2019). This indicates a limited zircon $\delta^{18}O$ range of 8.1–9.1 with an average value of 8.56 ± 0.17‰ for the Konglong trachytes, similar to those of the Konglong ultrapotassic enclaves (8.1–8.9‰ with an average value of 8.56 ± 0.26‰) (Hao et al., 2018).

3.2. Mineral compositions

The clinopyroxenes (Cpx) of the Konglong trachytes have variable MgO and FeO contents of 8.4–16.4, 3.8–15.0 wt%, respectively, with variable Mg# [Mg/(Mg + Fe)] of 50–89, and high CaO contents of 20.5–24.4 wt%, and thus are diopside and sahlite (Fig. 3a-b). The compositions of the Cpx are identified as $Wo_{43-49}En_{25-46}Fs_{6-26}$. These geochemical features distinguish them from the Cpx of the Sailipu mantle xenoliths (Liu et al., 2011), which is mainly endiopside with low CaO contents and high Mg# (Fig. 3a-b). This could likely suggest that the Cpx in the Konglong trachytes is phenocrystic rather than mantle xenocrystic. Besides, some Cpx phenocrysts show oscillatory zoning (Fig. 3c). For instance, a Cpx grain in the sample KL20–1 has core-mantle-rim Mg# values of 68, 86 and 67, respectively.

The micas of the Konglong trachytes are generally characterized by low Al_2O_3 (10.8–14.1 wt%) and variable TiO_2 (1.8–7.2 wt%), FeO (5.6–20.3 wt%) and MgO (13.2–25.2 wt%) contents with a wide range in Mg# (59–89), which are similar to the phlogopites (Phl) of the ultrapotassic rocks (e.g., TiO_2 = 1.6–9 wt%, Mg# = 62–92, Zhao et al., 2009), but distinct from the Phl with low TiO_2 and high Mg# in the mantle xenoliths (Liu et al., 2011) (Fig. 3d). According to the classification of Foster (1960), these mica phenocrysts in the Konglong trachytes are Mg-biotites and phlogopite (Fig. 3d).

The amphiboles (Amp) of the Konglong trachytes, based on the International Mineralogical Association's classification and the Fe^{3+} calculation proposed by Leake et al. (1997), belong to the calcic group [Ca_B (1.8–2.3) >1.5 atoms per formula unit (apfu)], and show $(Na + K)_A \geq 0.5$ apfu, Ti < 0.50 apfu. The Amp has high Si content with Si in formula >6 apfu and is classified as the magnesiohastingsite ($^{VI}Al < Fe^{3+}$)-pargasite ($^{VI}Al \geq Fe^{3+}$)-edenite series (Fig. 3e).

The alkali feldspars of the Konglong trachytes have high K_2O (5.9–17.4 wt%) and low Na_2O (0.2–5.7 wt%) and CaO (0–1.7 wt%) contents and are sandine with variable mole fraction of orthoclase (Or_{41-98}). The plagioclases of the Konglong trachytes are minor and generally show high CaO (6.5–10.4 wt%) and Na_2O (4.8–6.7 wt%) and low K_2O contents (0.8–1.6 wt%) with compositions of An_{32-52} (mole fraction of anorthite), and belong to andesine and labradorite (Fig. 3f).

Table 1
Major, trace elemental and Sr-Nd-Pb isotopic compositions for the Konglong trachytes.

Sample	KL01–1	KL01–2	KL02–1	KL02–2	KL02–4	KL02–5	KL03–1	KL03–2	KL03–3
SiO_2	61.95	63.29	62.61	61.20	61.38	62.01	61.44	61.04	56.49
TiO_2	1.10	1.00	1.01	1.05	1.00	1.07	1.28	1.04	1.50
Al_2O_3	15.81	15.09	15.56	15.18	15.27	15.51	14.91	14.69	15.14
Fe_2O_3T	5.24	4.55	4.74	5.41	5.27	4.74	5.34	4.80	6.17
MnO	0.10	0.08	0.10	0.09	0.08	0.08	0.09	0.10	0.12
MgO	1.98	2.08	1.69	2.55	2.32	2.28	2.11	2.62	3.07
CaO	3.27	3.35	3.48	3.73	3.97	3.43	3.17	4.45	5.30
Na_2O	2.92	2.83	3.41	3.11	3.07	3.35	2.58	3.06	3.11
K_2O	7.07	7.17	6.90	7.05	7.03	6.95	8.36	7.49	8.29
P_2O_5	0.56	0.57	0.51	0.64	0.60	0.57	0.73	0.70	0.81
LOI	2.06	0.78	0.24	1.08	0.29	0.71	0.15	0.24	0.41
Sc	10.5	10.0	9.63	10.8	11.0	10.3	11.7	10.2	14.9
V	80.4	70.7	75.3	88.4	86.9	79.3	97.0	81.0	118
Cr	203	153	258	246	240	106	245	226	274
Co	11.4	9.85	9.31	11.7	11.8	10.3	12.0	11.0	15.4
Ni	26.8	21.1	20.8	23.5	24.2	14.5	25.1	32.5	28.6
Cu	28.2	23.3	33.7	33.5	33.8	20.7	33.1	28.2	29.1
Zn	82.8	77.4	84.1	85.2	85.9	87.4	91.3	74.5	118
Ga	22.5	20.3	21.4	21.9	21.8	21.8	22.7	21.4	28.6
Ge	3.23	3.09	3.42	3.50	3.47	3.41	3.68	3.50	4.67
Cs	36.4	37.6	69.1	65.7	55.8	43.5	63.7	61.8	246
Rb	665	560	632	656	695	636	691	683	983
Ba	1883	1844	1899	1870	2214	2112	1999	2365	2316
Th	145	129	135	140	150	133	155	144	463
U	24.1	22.8	17.2	24.3	26.5	21.7	21.1	20.4	118
Nb	32.8	29.5	31.6	30.8	30.0	30.1	34.8	30.1	98.1
Ta	2.24	1.96	2.17	2.16	2.00	2.02	2.28	2.01	4.69
La	86.9	78.8	90.8	81.8	83.7	87.9	92.3	96.5	124.1
Ce	197	174	205	184	186	197	208	220	290
Pb	74.8	69.4	68.9	68.3	79.0	86.0	77.9	69.0	166
Pr	26.1	23.2	27.0	25.1	25.3	26.5	27.7	29.2	41.5
Sr	1410	1389	1253	1117	1306	1290	1395	1890	1935
Nd	109	97.0	112	107	108	111	116	123	165
Zr	558	516	476	499	514	439	627	531	1660
Hf	14.5	13.2	12.8	13.6	13.5	12.1	16.3	14.1	38.2
Sm	21.0	18.5	20.9	21.0	21.2	20.8	22.4	22.8	33.0
Eu	3.69	3.36	3.79	3.70	3.78	3.79	3.88	4.09	5.58
Gd	11.6	10.1	11.4	12.0	12.2	11.7	13.1	12.8	17.7
Tb	1.14	1.00	1.11	1.20	1.22	1.14	1.38	1.24	1.77
Dy	5.09	4.48	4.91	5.41	5.42	4.99	6.20	5.34	7.63
Y	20.8	18.2	19.3	22.0	21.6	19.8	25.8	21.3	31.4
Ho	0.83	0.73	0.79	0.88	0.88	0.80	1.02	0.86	1.21
Er	1.89	1.72	1.79	2.06	2.01	1.83	2.40	1.94	2.82
Tm	0.25	0.22	0.23	0.26	0.26	0.23	0.31	0.25	0.37
Yb	1.51	1.34	1.36	1.57	1.55	1.39	1.87	1.56	2.23
Lu	0.24	0.20	0.20	0.24	0.24	0.21	0.29	0.23	0.34
$^{143}Nd/^{144}Nd$	0.51208		0.51211				0.51208		0.51204
$^{87}Sr/^{86}Sr$	0.71280		0.71179				0.71349		0.71399
$^{206}Pb/^{204}Pb$	18.82		18.79				18.91		18.88
$^{207}Pb/^{204}Pb$	15.74		15.74				15.75		15.75
$^{208}Pb/^{204}Pb$	39.55		39.51				39.76		39.61
$^{147}Sm/^{144}Nd$	0.12		0.11				0.12		0.12
$^{143}Nd/^{144}Nd(i)$	0.51206		0.51209				0.51206		0.51202
εNd(t)	−10.69		−10.10				−10.71		−11.47
$^{87}Rb/^{86}Sr$	1.37		1.46				1.43		1.47
$^{87}Sr/^{86}Sr(i)$	0.71239		0.71135				0.71307		0.71355

Sample	KL03–4	KL03–5	KL03–6	KL03–7	KL17–2	KL18–1	KL19–1	KL19–2	KL20–2
SiO_2	59.09	60.95	59.31	61.09	60.25	59.22	61.01	59.67	67.82
TiO_2	1.11	1.03	1.11	1.07	1.17	1.50	1.49	1.08	0.69
Al_2O_3	15.20	14.57	15.45	14.85	14.63	16.59	15.14	15.25	14.11
Fe_2O_3T	5.17	4.88	5.18	5.29	5.25	5.61	6.10	5.61	3.54
MnO	0.11	0.10	0.10	0.11	0.10	0.07	0.18	0.12	0.08
MgO	2.88	2.68	2.64	2.52	2.75	1.61	2.17	2.65	1.26
CaO	5.08	4.38	4.50	3.87	5.01	1.76	2.58	4.66	2.51
Na_2O	2.89	3.24	3.08	2.90	2.84	1.86	2.42	3.11	3.07
K_2O	7.79	7.45	8.04	7.74	7.29	10.84	8.01	7.31	6.58
P_2O_5	0.68	0.71	0.59	0.55	0.74	0.94	0.90	0.54	0.34
LOI	0.20	0.22	0.24	0.34	0.20	1.02	1.53	0.72	0.35
Sc	12.4	10.1	12.4	11.6	11.9	14.2	13.8	10.5	6.70
V	92.8	80.8	96.8	95.5	95.8	107	121	89.0	51.2
Cr	151	222	168	341	205	116	135	99	319
Co	12.6	11.8	12.3	12.8	13.0	15.8	15.2	12.0	6.97
Ni	23.2	35.3	22.1	32.0	25.2	17.0	25.4	15.7	25.2

Table 1 (*continued*)

Sample	KL03–4	KL03–5	KL03–6	KL03–7	KL17–2	KL18–1	KL19–1	KL19–2	KL20–2
Cu	19.5	25.4	26.0	45.4	30.1	26.1	27.3	20.9	37.3
Zn	79.7	72.8	81.4	102	80.1	110	92.9	84.4	66.2
Ga	22.4	20.8	24.0	25.9	21.5	24.3	26.0	21.8	19.3
Ge	3.65	3.60	3.77	4.07	3.84	3.53	4.27	3.75	2.56
Cs	67.9	44.5	76.6	111	34.0	10.0	21.9	21.6	60.9
Rb	704	647	811	929	673	993	862	785	676
Ba	2297	2250	2196	2062	2363	2333	2258	2045	1660
Th	171	138	192	226	140	170	159	133	137
U	22.9	20.9	27.2	28.2	25.4	37.1	26.8	22.0	18.3
Nb	35.4	29.0	40.4	45.7	30.8	37.1	36.7	31.5	23.1
Ta	2.31	1.92	2.59	2.93	2.08	2.49	2.40	2.10	1.43
La	88.6	93.2	95.2	109.5	98.6	87.4	96.5	87.7	71.8
Ce	204	214	221	245	232	205	228	207	153
Pb	94.4	58.9	67.9	111	65.9	70.5	59.8	61.6	72.3
Pr	27.3	28.5	29.7	32.0	31.4	27.4	32.3	29.0	19.2
Sr	1590	1752	1403	1404	2013	1755	1801	1448	1333
Nd	116	119	124	134	134	118	139	125	75.4
Zr	660	523	726	826	528	640	628	532	416
Hf	17.4	13.9	18.7	21.0	14.1	17.2	16.3	14.3	11.3
Sm	23.3	22.2	24.6	25.6	25.2	24.8	27.3	24.0	13.7
Eu	4.13	3.90	4.32	4.33	4.45	4.35	4.60	4.17	2.44
Gd	13.3	12.4	14.1	14.6	13.7	14.4	15.0	13.2	7.78
Tb	1.35	1.21	1.42	1.47	1.33	1.49	1.48	1.30	0.76
Dy	6.10	5.25	6.26	6.55	5.87	6.50	6.41	5.70	3.35
Y	24.5	21.0	25.5	26.8	23.0	25.2	24.9	22.1	14.1
Ho	0.98	0.82	1.00	1.04	0.93	1.03	1.01	0.90	0.55
Er	2.28	1.91	2.30	2.41	2.12	2.34	2.24	2.01	1.31
Tm	0.30	0.24	0.30	0.32	0.28	0.29	0.28	0.26	0.18
Yb	1.76	1.47	1.77	1.92	1.62	1.74	1.62	1.51	1.09
Lu	0.27	0.23	0.27	0.29	0.25	0.26	0.24	0.23	0.17
$^{143}Nd/^{144}Nd$	0.51208			0.51206		0.51208	0.51209		
$^{87}Sr/^{86}Sr$	0.71330			0.71434		0.71237	0.71230		
$^{206}Pb/^{204}Pb$	18.85			18.88		18.95	18.95		
$^{207}Pb/^{204}Pb$	15.75			15.75		15.75	15.75		
$^{208}Pb/^{204}Pb$	39.61			39.63		39.79	39.80		
$^{147}Sm/^{144}Nd$	0.12			0.12		0.13	0.12		
$^{143}Nd/^{144}Nd(i)$	0.51206			0.51205		0.51207	0.51207		
εNd(t)	−10.74			−11.03		−10.64	−10.57		
$^{87}Rb/^{86}Sr$	1.28			1.92		1.64	1.39		
$^{87}Sr/^{86}Sr(i)$	0.71292			0.71376		0.71189	0.71189		

3.3. Whole-rock major and trace elemental and Sr-Nd-Pb isotopic compositions

The Konglong trachytes, including 18 samples from this study, 11 samples from Chen et al. (2010) and 4 samples from Hao et al. (2019), display high SiO_2 and ($K_2O + Na_2O$) contents of 56.5–67.8 wt% and 9.6–12.7 wt%, respectively, and are alkaline (Fig. 4a). On a K_2O vs. SiO_2 plot (Fig. 4b), they show the shoshonitic characteristic due to their high K_2O contents (6.6–10.8 wt%). They have slightly low Na_2O contents of 1.9–3.4 wt% and thus high K_2O/Na_2O values (2.0–5.8), indicating their potassic-rich character. However, the Konglong trachytes clearly deviate from the fields of the southern Tibetan ultrapotassic (Guo et al., 2015; Turner et al., 1996; Zhao et al., 2009) and northern Tibetan potassic rocks (Ding et al., 2003; Guo et al., 2006; Ou et al., 2018; Williams et al., 2004), on the total alkali-silica (TAS) discrimination diagram (Fig. 4a). Therefore, here we refer to them as the high-silica potassic rocks (HSPs) and similar coeval rocks occurred widely in the Lhasa block (e.g., the Xungba and Yangying areas) (Fig. 1) (Liu et al., 2014; Miller et al., 1999; Nomade et al., 2004).

The Konglong trachyte samples have TiO_2 (0.69–1.54 wt%), Al_2O_3 (13.8–16.6 wt%), Fe_2O_3 (3.5–6.2 wt%), MnO (0.05–0.18 wt%), CaO (1.4–5.3 wt%), Na_2O (1.9–3.4 wt%) and P_2O_5 (0.04–0.94 wt%) contents. On major-element Harker diagrams (Fig. 4), K_2O, MgO, TiO_2, CaO, P_2O_5 and Fe_2O_3 show decreasing trends with increasing SiO_2, whereas Na_2O and Al_2O_3 show approximately flat trends with elevated SiO_2. They generally plot between the fields of ultrapotassic rocks (lavas and enclaves) and felsic rocks (e.g., the post-collisional adakites in southern Lhasa block (SLB) and Xungba HSPs) on major-element (Na, Fe, Al, Mg, Ti, Ca and P) Harker diagrams (Fig. 4c-i). Notably, on a plot of SiO_2 vs. K_2O, they only plot between the ultrapotassic rocks and Xungba HSPs (rather than adakites), due to the low K_2O contents of the SLB adakites (Fig. 4b).

On the chondrite-normalized REE (rare earth element) diagram (Fig. 5a), the Konglong trachytes show right-sloping patterns and clear fractionation between light REEs (LREEs) and heavy REEs (HREEs) with $(La/Yb)_N = 16–49$. HREEs are more highly fractionated with $(Gd/Yb)_N = 5.8–7.7$, than LREEs, which show flat patterns with $(La/Sm)_N = 1.4–3.7$. They exhibit moderately negative Eu anomalies ($Eu/Eu^* = 0.69–0.75$). The Konglong trachytes have lower but approximately parallel REE distribution patterns (particularly, the flat LREEs) relative to the ultrapotassic lavas and enclaves. They clearly differ from the Xungba HSPs, which generally show significant fractionated LREEs. They are also distinct from the SLB post-collisional adakites, which have clear fractionated LREEs and no negative Eu anomalies. Primitive mantle-normalized trace-element distribution patterns of the Konglong trachytes (Fig. 5b) are characterized by the enrichment of large ion lithophile elements (LILEs) (e.g., Rb, Th, U, Pb, and Ba), and the depletion of Sr and high field strength elements (HFSEs) (e.g., Nb, Ta). The negative Sr anomalies distinguish the Konglong trachytes from the SLB post-collisional adakites with positive Sr anomalies.

The Konglong trachytes have slightly variable and enriched Sr—Nd isotope compositions with initial $^{87}Sr/^{86}Sr$, $^{143}Nd/^{144}Nd$ ratios of 0.7114–0.7138 and 0.51197–0.51209, respectively, and εNd($t = 21$ Ma) of −12.5 to −10.1 (Fig. 6a). They show slightly more enriched Sr—Nd isotope compositions than the Konglong enclaves. The Konglong trachytes exhibit highly radiogenic Pb isotopic signatures with

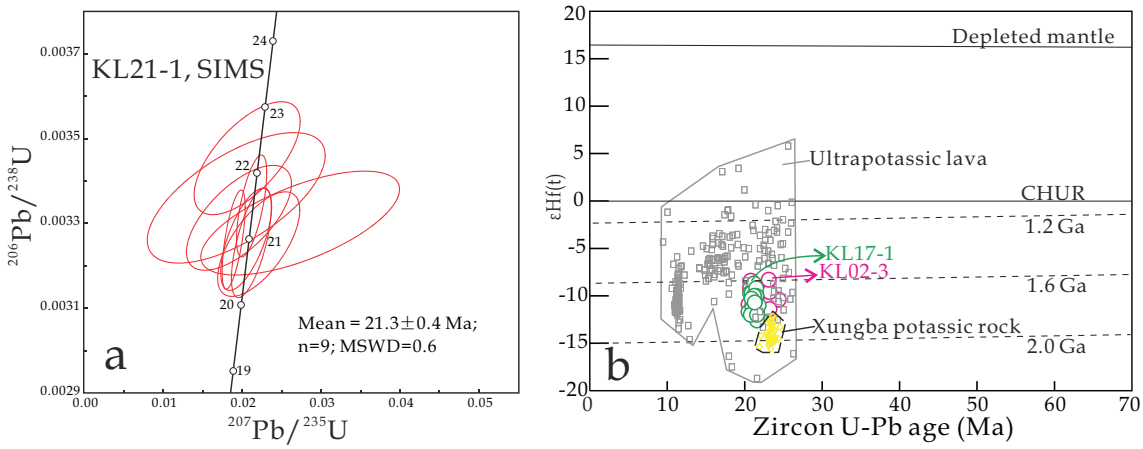

Fig. 2. (a) SIMS zircon U—Pb dating result for the Konglong trachyte sample KL21–1. Besides, zircon U—Pb ages for samples KL17–1 (LA + SIMS), KL21–1 (LA) and KL02–3 (SIMS) can be found in Hao et al. (2018, 2019). (b) Zircon Hf isotopic compositions for the Konglong trachyte samples KL17–1 and KL02–3. Zircon Hf isotope data for the ultrapotassic lavas and Xungba potassic rocks are from Liu et al. (2014, 2017).

$^{206}Pb/^{204}Pb$ = 18.79–18.95, $^{207}Pb/^{204}Pb$ = 15.74–15.75, $^{208}Pb/^{204}Pb$ = 39.51–39.79 (Fig. 6b-c), which are in common with the post-collisional ultrapotassic lavas and enclaves and Xungba HSPs but distinct from the SLB post-collisional adakites.

4. Discussion

4.1. Genesis of the Konglong trachytes

4.1.1. A lower crust origin?

The widespread post-collisional adakites in the SLB of southern Tibet were widely suggested to have originated from Lhasa thickened juvenile lower crust (e.g., Chung et al., 2003; Hou et al., 2004; Zhang et al., 2014). Likewise, the Konglong Miocene trachytes, with high SiO_2 (56.5–67.8 wt%) and low MgO (1.3–3.0 wt%) contents and high La/Yb (22–67) and Sr/Y (51–109) values (Fig. 5c-d), were previously considered to have originated from the thickened lower crust (Chen et al., 2010). However, significant geochemical differences occurred between the Konglong trachytes and the SLB post-collisional adakites: (1) The adakites commonly have low (K_2O + Na_2O) and K_2O contents and are sub-alkaline and calc-alkaline, while the Konglong trachytes have high (K_2O + Na_2O) and K_2O contents and are alkaline and shoshonitic (Fig. 4); (2) The adakites have variable (slightly enriched to depleted) Sr—Nd isotopic compositions and overall depleted zircon Hf isotopic compositions, which are often ascribed to the SLB juvenile crust source (Zhang et al., 2014). The Konglong trachytes, however, have more

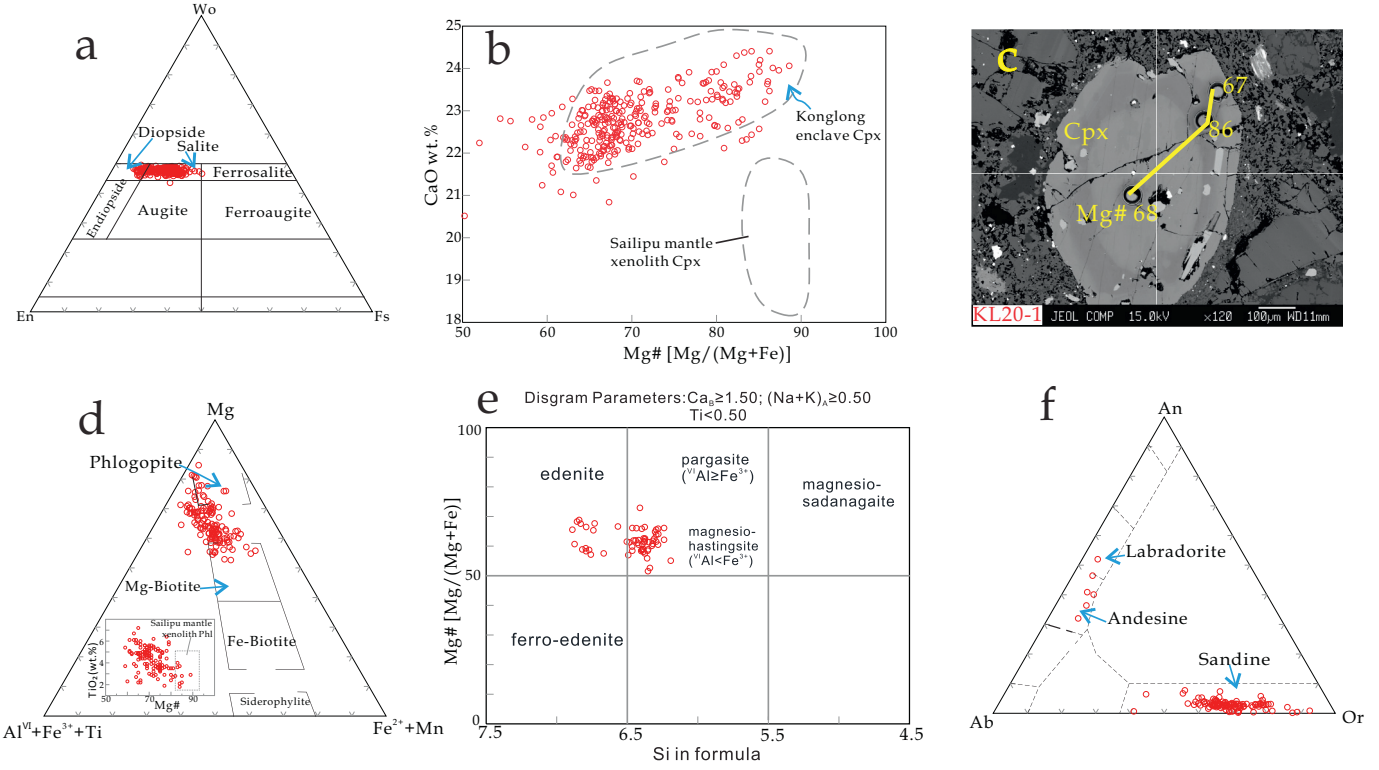

Fig. 3. Mineral compositions for the Konglong trachytes. (a) A Wo-En-Fs diagram for clinopyroxene (Cpx). (b) Mg# vs. CaO for Cpx. (c) The oscillatory zoning of Cpx phenocrysts. (d) Plot of micas in Mg-(Fe^{2+} + Mn)-(Al^{VI} + Fe^{3+}+Ti) (apfu) diagram. The inset compares the micas to mantle phlogopites (Phl). (e) Classification of calcic amphiboles with parameters: Ca_B ≥ 1.50, $(Na + K)_A$ ≥ 0.50, and Ti < 0.50. (f) A Or-Ab-An diagram for feldspar. The Cpx and Phl compositions of the Sailipu mantle xenoliths are from Liu et al. (2011).

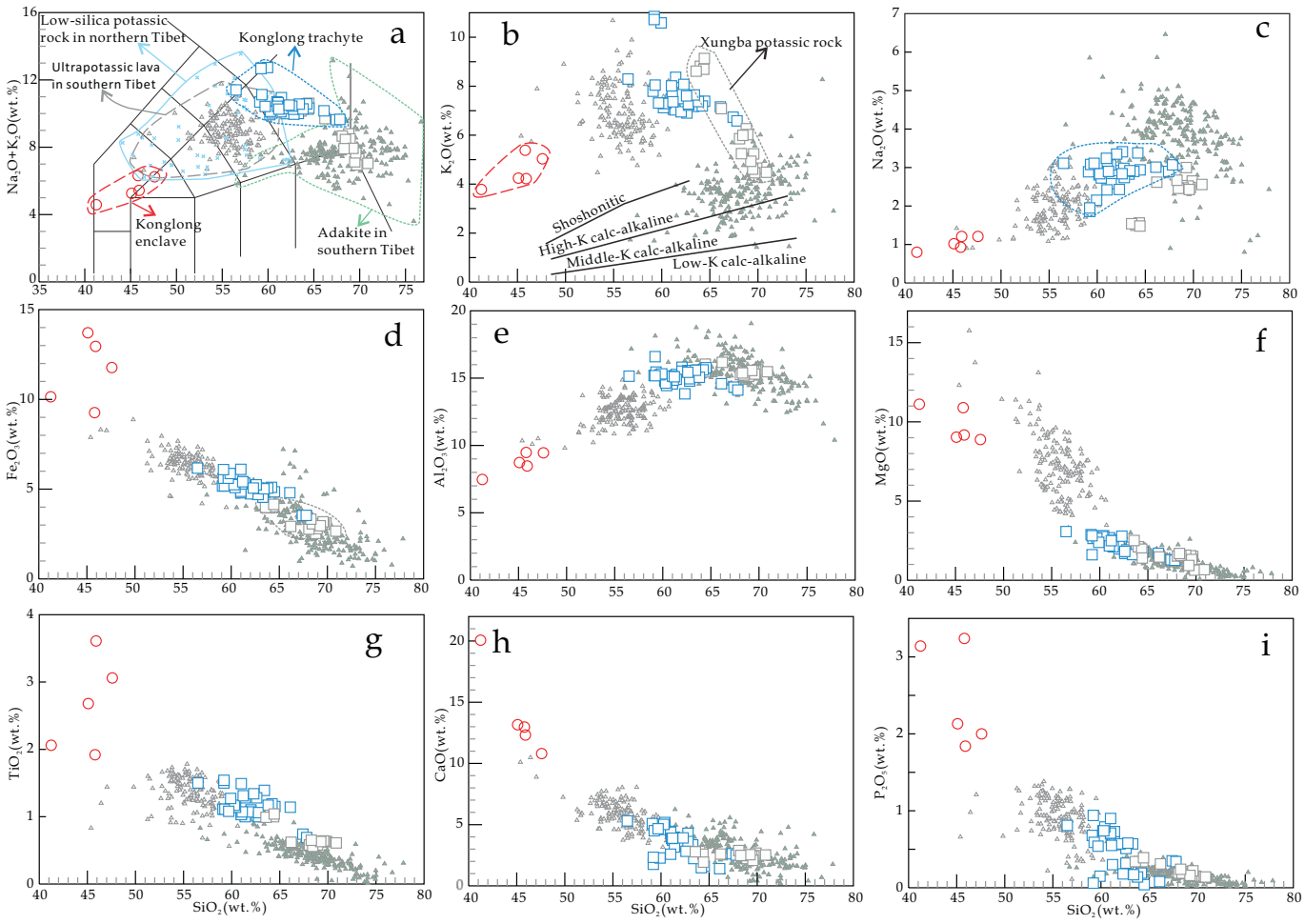

Fig. 4. Major-element compositions for the Konglong trachytes. (a) TAS diagram; (b-i) Harker diagrams. The potassic rocks of northern Tibet are from Ding et al. (2003) and Guo et al. (2006). The ultrapotassic lavas and enclaves of southern Tibet are from Hao et al. (2018, 2019) and references therein. The Xungba potassic rocks are from Liu et al. (2014).

enriched Sr-Nd-Hf isotopes than the adakites (Fig. 6); (3) The Pb isotopic values (e.g., $^{206}Pb/^{204}Pb$ and $^{208}Pb/^{204}Pb$) of the Konglong trachytes are also clearly higher than those of the adakites (Fig. 6); (4) The Konglong trachytes show high HREE (e.g., Yb) and Y contents, and significantly negative Eu and Sr anomalies, which are clearly different from those of the adakites (low Y and Yb, negligible Eu- and positive Sr-anomalies) (Fig. 5). Therefore, the Konglong trachytes were unlikely derived by partial melting of a juvenile crust.

Recently, a thickened ancient Lhasa lower crust origin was invoked to explain the high K_2O contents, high La/Yb ratios and enriched Sr-Nd-Hf isotopes of some HSPs in the Lhasa block (e.g., the Xungba HSPs) (Liu et al., 2014). Moreover, plagioclase fractionation during generation of the Xungba HSPs can account for their variably negative Eu and Sr anomalies, lower Sr/Y ratios and slightly higher Yb contents, given that Sr and Eu, and Yb are compatible and incompatible in plagioclase, respectively. Actually, the Xungba HSPs show slightly increasing Yb and nearly constant Y contents with increasing SiO_2 (Fig. 7a-b), indicating that the parental or less fractionated magmas had low Yb and Y contents consistent with a thickened crust source. The Konglong trachytes also have high K_2O contents and La/Yb ratios, enriched Sr-Nd-Hf isotopes and negative Eu and Sr anomalies. However, a genetic model involving partial melting of a thickened ancient crust cannot account for their generation. The trachytes show well-developed negative correlation trends for SiO_2 vs. Y, and Yb (Fig. 7a-b) and the samples with lower SiO_2 have higher Yb and Y contents. These correlations argue against partial melting of a thickened ancient crust origin and subsequent plagioclase fractionation for their generation.

Actually, the flat LREE distribution patterns (i.e., low La/Sm ratios) of the Konglong trachytes are one of the most significant geochemical features that distinguish them from the SLB post-collisional adakites and Xungba HSPs. On a La/Yb vs. Sm/Yb plot (Fig. 7c), the adakite and Xungba HSP samples fall along modelled trends for partial melting of the garnet-bearing amphibolite, amphibole-bearing eclogite and eclogite, consistent with their thickened crust origin. However, the Konglong trachytes show elevated Sm/Yb at given La/Yb ratios, i.e., lower La/Sm, clearly deviating from the modeling melting curves and ruling out a lower crust source for their origin.

4.1.2. Magma mixing

The significant petrogenetic and geochemical differences between the Konglong trachytes and crust-derived rocks of the Lhasa block (e.g., SLB post-collisional adakites and Xungba HSPs) rule out a lower crust origin for the trachytes. Instead, a close relationship between the Konglong trachytes and the ultrapotassic rocks is strongly suggested by their similar REE and trace-element distribution patterns, and bulk-rock Sr-Nd-Pb and zircon O isotopes. The similarities probably indicate a significant contribution of ultrapotassic magmas to the Konglong trachytes. Furthermore, high Mg# values (up to 89) of the clinopyroxene (Cpx) phenocrysts in the Konglong trachytes also indicate the involvement of ultrapotassic magmas during their generation. Calculated Mg# of parental liquids in equilibrium with the Cpx (Wood and Blundy, 1997) extends up to 70, coinciding with those of mantle-derived magmas. Indeed, several recent studies have identified important contributions of ultrapotassic magmas to some post-collisional HSPs in

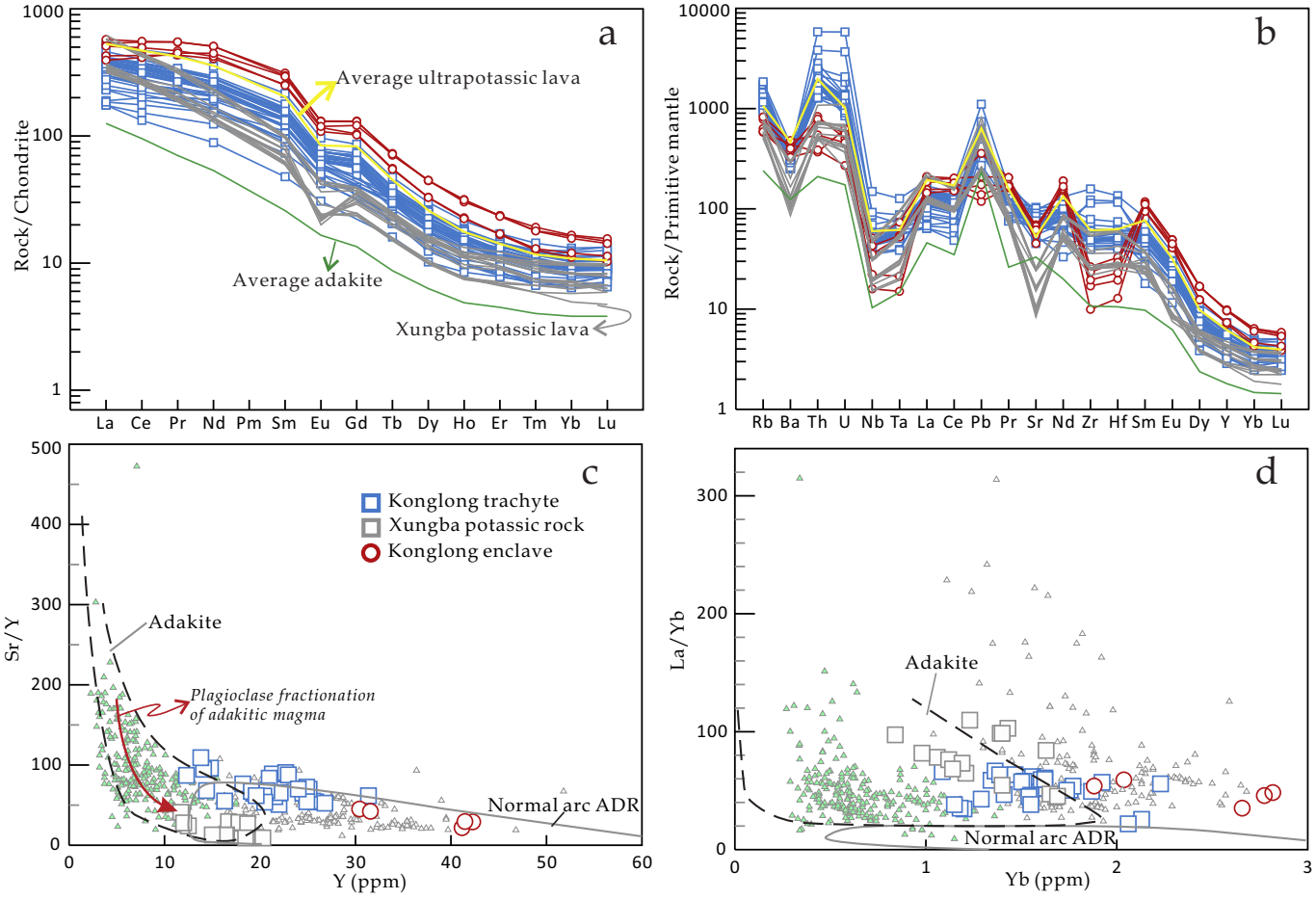

Fig. 5. (a) REE distribution patterns and (b) trace-element spider diagrams for the Konglong trachytes. (c) Y vs. Sr/Y. (d) Yb vs. La/Yb. Chondrite and primitive mantle values are from Sun and McDonough (1989). The trend of plagioclase fractionation of adakitic magmas is from Liu et al. (2014).

the Lhasa block (Liu et al., 2017; Zhang et al., 2017). For example, Zhang et al. (2017) proposed that the Yangying HSPs formed via AFC of primitive ultrapotassic magmas. In this study, we prefer to suggest that mixing between crustal and ultrapotassic magmas, rather than (A)FC of ultrapotassic magmas, was responsible for generation of the Konglong trachytes, based on the following evidence.

The Konglong trachytes have very similar Sr-Nd-Pb isotopes and approximately parallel REE distribution patterns to the Konglong ultrapotassic enclaves (Figs. 5-6), yet, they may not be the differentiation products of ultrapotassic magmas in a nearly closed system. It is generally accepted that an evolved magma (except for a highly fractionated magma) relative to the parental magma would contain higher contents of the incompatible elements. The Konglong trachytes show lower incompatible element contents than the Konglong ultrapotassic enclaves (Fig. 5), inconsistent with their generation by FC of ultrapotassic magmas.

Macpherson et al. (2006) suggested that basaltic magmas could evolve into high-La/Yb and –Sr/Y rocks by fractional crystallization of a garnet-bearing assemblage. Increasing studies (e.g., Davidson et al., 2007; Tang et al., 2018) have recently suggested that garnet fractionation could be a common process during magma differentiation at high pressure. Indeed, the equilibrium and fractional crystallization experiments have determined that garnet can crystallize from basaltic magmas at a high pressure (e.g., 1.0–1.2 Gpa) in the lower crust or upper mantle (e.g., Ulmer et al., 2018; Müntener et al., 2001; Müntener and Ulmer, 2006, 2018). For instance, Ulmer et al. (2018) determined experimentally that fractional crystallization of the high-Mg basalt under oxidizing conditions evolves through fractionation of early olivine, Cpx, orthopyroxene, spinel, and Amp at 1200–980 °C, followed by garnet and plagioclase at 950 °C. However, a genetic model of high-pressure fractional crystallization (involving garnet) could not well explain the formation of the Konglong trachytes. Due to the HREE enrichment in garnet, garnet fractionation would result in the increase of Dy/Yb with differentiation (e.g., increasing SiO_2 contents) (Davidson et al., 2007; Macpherson et al., 2006; Tang et al., 2018). Instead, the Konglong trachytes display a negative covariation between Dy/Yb and SiO_2 (Fig. 7d), which indicates that they were unlikely produced by high-pressure fractional crystallization of basaltic magmas. Differentiation of the shallow, plagioclase-amphibole assemblage (Castillo et al., 1999) from basaltic magmas was also unable to produce the Konglong trachytes. In particular, the removal of these phases would produce concave-upwards patterns between the middle and heavy REEs (Macpherson et al., 2006), which are absent in the Konglong trachytes.

Actually, compared to the ultrapotassic enclaves, the Konglong trachytes have lower incompatible trace-element contents and slightly more enriched Sr—Nd isotopes, indicating that crustal components were involved in their generation. The oscillatory zoning of some Cpx phenocrysts strongly suggests that a mixing process between crustal and ultrapotassic magmas, rather than crustal assimilation, should play a key role in generating the Konglong trachytes.

As discussed above, the Konglong trachyte samples had plotted between the fields of the ultrapotassic enclaves and Xungba HSPs on major-element (Na, Fe, Al, Mg, Ti, Ca, P, K) Harker diagrams, consistent with mixing between mantle-derived and ancient crust-derived magmas. Besides, compared to the crustal end-member (low Y and Yb; high SiO_2 and La/Yb), ultrapotassic magmas have lower SiO_2, higher Y, Yb and similar La/Yb (Fig. 5c-d). Thus, their mixing can well explain

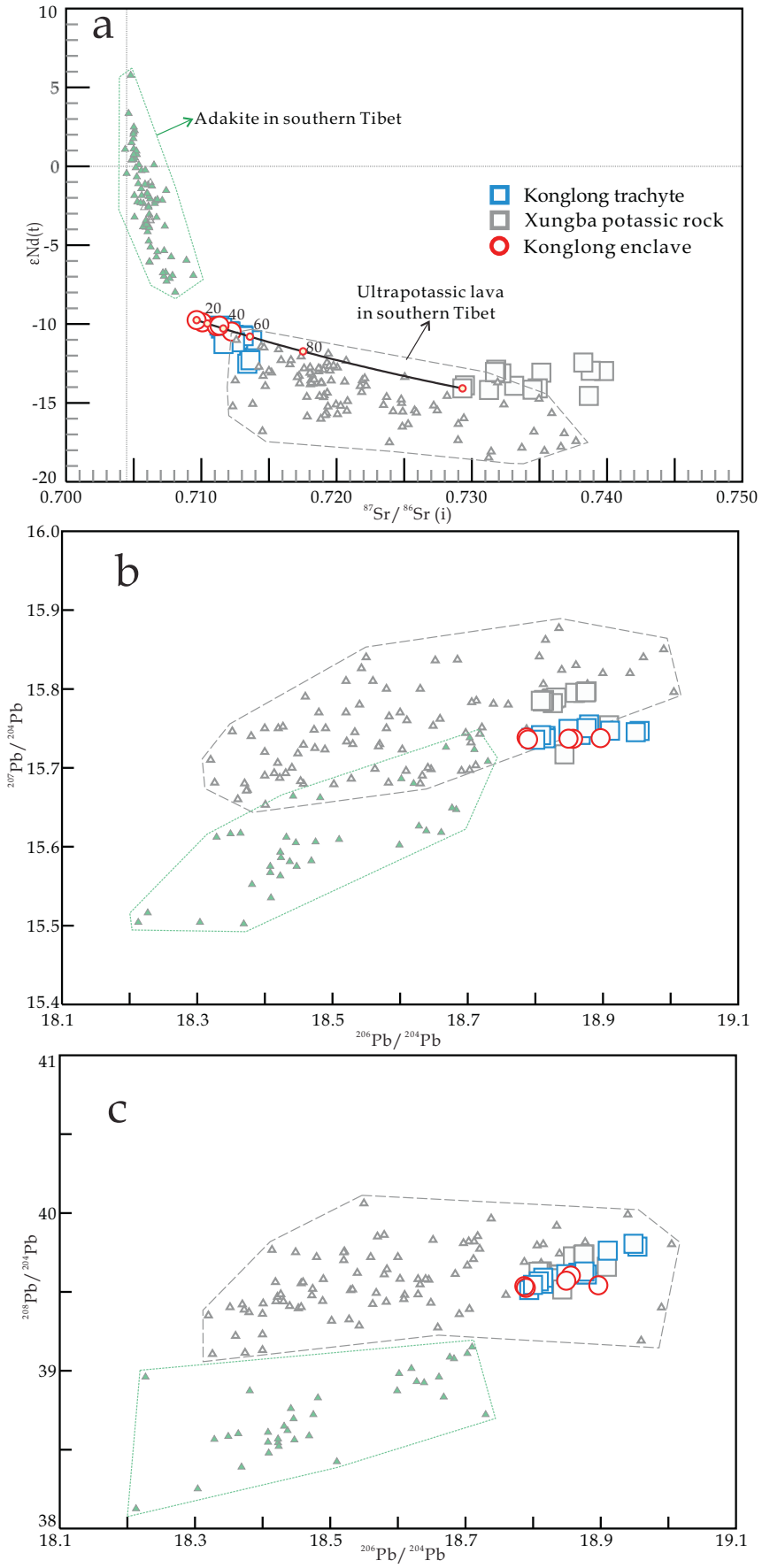

Fig. 6. Bulk-rock Sr-Nd-Pb isotopes for the Konglong trachytes. The curve in (a) shows the mixing trend between the ultrapotassic (KLBT02) and ancient crust-derived magmas (Xungba potassic lava sample 10XB04).

the negative covariation trends of Yb and Y vs. SiO_2 (Fig. 7a-b), and high La/Yb ratios along with high Y and Yb contents (Fig. 5c-d). Furthermore, mixing of thickened crust-derived (i.e., Xungba HSPs) and ultrapotassic magmas with low La/Sm can readily explain the weak fractionation of the LREEs (i.e., low $(La/Sm)_N$), one of the most distinctive features, for the Konglong trachytes (Fig. 7c). In addition, both the ultrapotassic rocks and Xungba HSPs have enriched zircon Hf (Fig. 2) and O isotopes (Hao et al., 2018; Liu et al., 2014), comparable to those of the Konglong trachytes. Their mixing thus can produce the Hf—O isotopes of the Konglong trachytes. Moreover, the Konglong trachytes have Sr—Nd isotopic compositions between those of the ultrapotassic enclaves and Xungba HSPs. Simple modeling result shows that mixing of ultrapotassic and 20–60% crustal magmas can produce the Sr—Nd isotope compositions of the Konglong trachytes (Fig. 6a).

Collectively, we suggest that the Konglong high-silica potassic rocks (trachytes) were generated by mixing of mantle-derived ultrapotassic and thickened ancient crust-derived magmas. Combined with the Xungba and Yangying HSPs (Liu et al., 2014; Zhang et al., 2017), we suggested that post-collisional high-silica potassic rocks in the Lhasa block should have variable genetic mechanisms involving melting of crustal sources, AFC of basaltic magmas and crust- and mantle-derived magma mixing.

4.2. Post-collisional geodynamics of the Lhasa block

Following the initial India-Eurasia (India-Lhasa) collision in the early Cenozoic (65–55 Ma) and Neo-Tethyan oceanic slab breakoff at 50–45 Ma, the Himalayan-southern Tibetan collision zone converted into a post-collisional intra-continental setting with Indian continental subduction beneath the Lhasa block (Chung et al., 2005; DeCelles et al., 2011). Subduction segmentation of the Indian plate (Hao et al., 2019; Wang et al., 2018) appears likely because geophysical data have recently shown that the subduction angle of the northward Indian plate beneath southern Tibet increases from west to east (Chen et al., 2015). The spatial variation in magmatism and mineralization throughout the Lhasa block (Wang et al., 2018) is also consistent with the effects of subduction segmentation. Indian plate steep subduction for a short distance beneath the eastern Lhasa block (ELB) (east of 87°E) is consistent with the spatial distribution of the ELB post-collisional magmatism, which was restricted to the ELB southern margin (Fig. 1). In contrast, Indian plate flat subduction beneath the western Lhasa block (WLB) (west of 87°E) produced the WLB ~45–25 Ma magmatic gap (Chung et al., 2005). Subsequent renewed potassic and ultrapotassic magmatism (25–8 Ma) in the WLB was contemporaneous with the onset of the N-S extension-related tectonics (e.g., the main central thrust (MCT), the South Tibetan detachment system (STDS) and the Kailas basin) (DeCelles et al., 2011) and the Konglong A-type magmatism (Hao et al., 2019) of the Himalayan-southern Tibetan orogen. Hao et al. (2019) suggested that these diverse events straddled both the Himalaya and Lhasa blocks can be reconciled with the foundering of the northward subducted Indian plate (DeCelles et al., 2002, 2011). In this scenario, Indian plate subducted at a low-angle and reached the region beneath the central WLB during 45–25 Ma (Hao et al., 2018). After ~25 Ma, foundering of the flat Indian plate caused significant N-S extension,

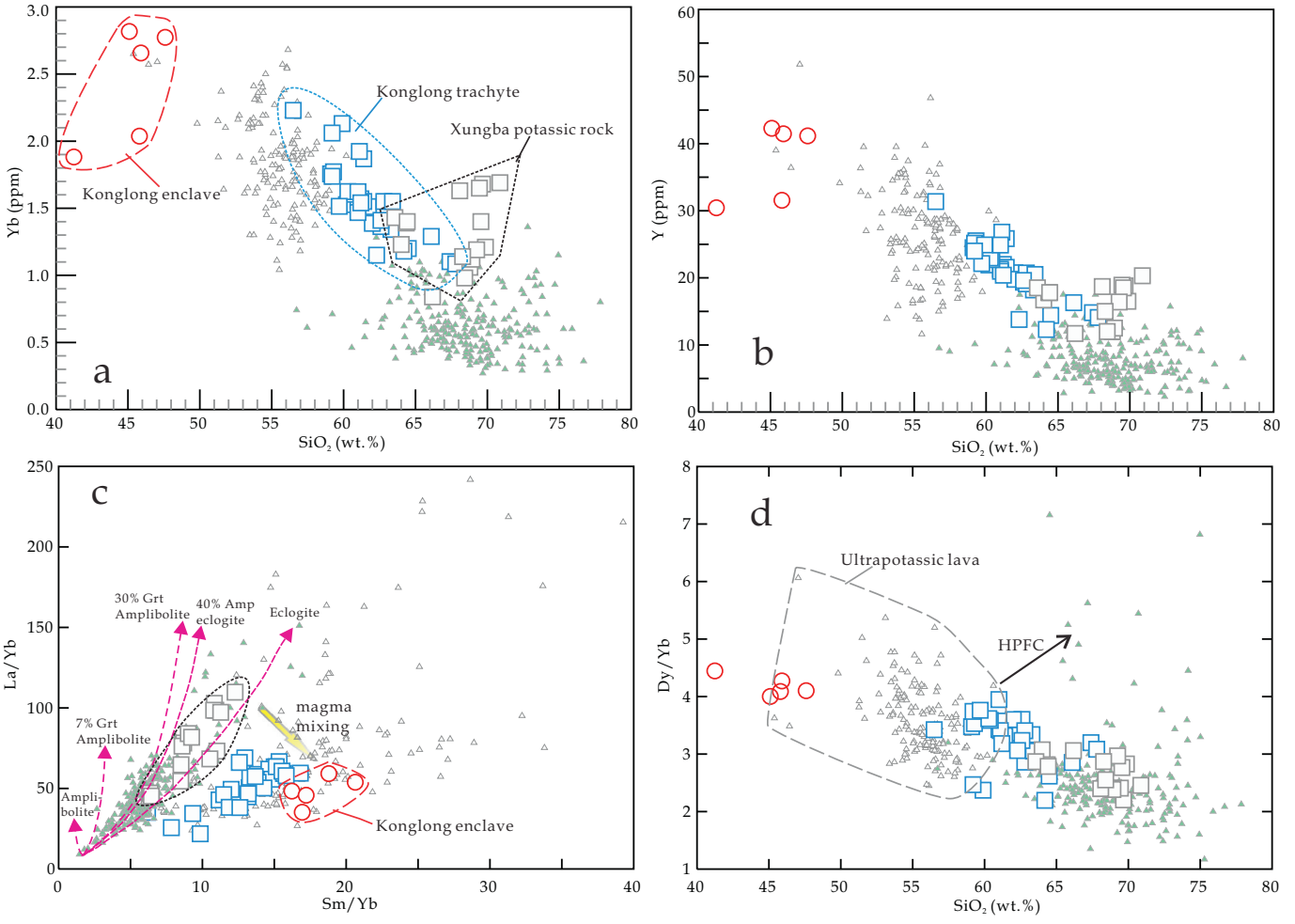

Fig. 7. (a-b) SiO_2 vs. Yb and Y, respectively, for the Konglong trachytes. (c) La/Yb vs. Sm/Yb. The modeling curves of partial melting of the garnet-bearing amphibolite, amphibole-bearing eclogite and eclogite are from Liu et al. (2017). (d) Dy/Yb vs. SiO_2. The high-pressure fractional crystallization (HPFC) trend is from Macpherson et al. (2006).

ultrapotassic and leucogranitic magmatism. The ancient crust of southern Tibet then melted and mixed with ultrapotassic magmas to form the Konglong HSPs, as a result of underplating of ultrapotassic magmas.

4.3. Crustal reworking of southern Tibet during Indian continental subduction

The Himalayan-southern Tibetan orogen, characterized by the thickest continental crust on Earth (60–80 km) (Kind et al., 1996), is one of the most prominent continent-continent collision zones in the Cenozoic, and resulted from Neo-Tethyan oceanic and Indian continental subduction (Yin and Harrison, 2000). Deciphering the orogen's crustal evolution (growth and reworking) is of significant importance for understanding other continent-continent collision zones on Earth. Numerous studies have clarified the crustal growth of southern Tibet during Neo-Tethyan oceanic subduction: (1) significant juvenile crustal growth occurred in the southern Lhasa block (SLB), but not in the CLB, by mantle- or oceanic slab-derived magma accretion (Zhang et al., 2010; Zhu et al., 2011, 2018); (2) The CLB ancient crust was weakly affected by Neo-Tethyan oceanic subduction and evolved mainly via crustal remelting (Zhou et al., 2017; Zhu et al., 2009, 2011).

Crustal reworking of the Himalayan-southern Tibetan orogen during Indian continental subduction was widely considered to be dominated by partial melting of the subducted Indian continental crust during *syn*-exhumation and post-collisional crustal thinning, as recorded by the Cenozoic adakitic and leucogranitic magmatism in the Himalaya block, respectively (Hou et al., 2012; Wu et al., 2015; Zeng et al., 2011; Zhang et al., 2004). Post-collisional mixing between mantle-derived ultrapotassic and thickened juvenile crust-derived adakitic magmas recently identified in the SLB of southern Tibet (Sun et al., 2018; Wang et al., 2018; Yang et al., 2015) indicates that magma underplating and crust-mantle mixing was likely an additional mechanism for crustal reworking in this orogen. Identifying magma mixing in the CLB provides crucial evidence for this hypothesis, particularly because Indian continent subduction beneath the CLB had initiated by at least ca. 21 Ma (Hao et al., 2018).

Post-collisional magma mixing of the CLB is clearly identified in this study. Integrated studies of mineral compositions, whole-rock major-, trace-element geochemistry, and Sr-Nd-Pb-Hf-O isotopes clearly suggest that the Konglong trachytes were generated by mixing of mantle-derived ultrapotassic and thickened ancient crust-derived magmas. This evidence suggests that matter and energy transfer from the mantle to the crust (i.e., melting of thickened ancient crust induced by injection of ultrapotassic magmas and subsequent mantle-crust mixing) played a key role in crustal reworking of the CLB during Indian continental subduction. In addition, the Konglong ultrapotassic enclaves also indicate ultrapotassic underplating beneath the Lhasa deep crust (Hao et al., 2018), which caused crustal melting and magma mixing to generate the host magmas (trachytes). The underplated ultrapotassic intrusions were then captured as enclaves by host trachytic magmas.

Therefore, crust-mantle mixing was likely a common post-collisional crustal reworking process throughout southern Tibet (both the SLB and CLB). Based on the collective data, we conclude that crustal evolution of the Himalayan-southern Tibetan orogen involved: (1) Neo-Tethyan oceanic subduction-induced juvenile continental crustal growth of the SLB but not of the CLB; (2) in addition to partial melting of the subducted Indian continental crust, magma underplating beneath the obducted continent (injection of ultrapotassic magmas into juvenile and ancient crust of the SLB and CLB, respectively) and subsequent crustal melting and crust-mantle mixing was an additional effective mechanism for crustal reworking in the collisional zone. Post-collisional crustal reworking of southern Tibet was likely controlled by Indian plate flat subduction and subsequent foundering beneath the Lhasa block.

Post-collisional ultrapotassic magmatism is widely distributed along the Alpine-Himalayan orogenic belt, e.g., in the Western Mediterranean Region (Conticelli et al., 2009), the Turkish-Iranian plateau (Pang et al., 2013), and the southern Tibetan plateau (Chung et al., 2005). Furthermore, ultrapotassic rocks are generally found intimately associated, in space and time, with potassic/shoshonitic or calc-alkaline rocks (e.g., Conticelli et al., 2009; Miller et al., 1999), similar to the present case. Therefore, we speculate that crust-mantle mixing (i.e., the matter and energy transfer from the mantle to the crust) may well have played a key role in crustal reworking along the full length of the Alpine-Himalayan orogenic belt.

5. Conclusions

The Konglong Miocene trachytes in the central Lhasa block of the southern Tibetan plateau were generated by mixing between enriched mantle-derived ultrapotassic and thickened ancient lower crust-derived magmas. Considering post-collisional magma mixing recently identified in the southern Lhasa block, we proposed that magma underplating and subsequent mantle-crust interaction has been widespread and important processes for crustal reworking in southern Tibet during Indian continental subduction. This reworking is ascribed to Indian plate flat subduction and subsequent foundering during the post-collisional stage. Taking into account the Cenozoic magmatism in the Himalaya block, we suggested that, in addition to partial melting of the subducted continental crust during the syn-exhumation and post-collisional crustal thinning, magma underplating and subsequent crust-mantle mixing beneath the obducted continent also played an important role in crustal reworking of the collisional zone.

Acknowledgments

We thank Editor Professor Michael Roden, Professor Antonio Castro, and an anonymous reviewer for their constructive comments, which significantly improved our paper. The data supporting the conclusions can be found in the Supporting Information or are available by request from the corresponding author. Financial support was provided by Strategic Priority Research Program (A) of Chinese Academy of Sciences (CAS) (XDA2007030402), National Natural Science Foundation of China (91855215, 41630208, 41802048), the Second Tibetan Plateau Scientific Expedition and Research (STEP) (2019QZKK0702), the Key Program of the Chinese Academy of Sciences (QYZDJ-SSW-DQC026), the National Key R & D Program of China (No. 2016YFC0600407), the Key Program of Guangzhou City (No. 201604910124) and the Guangzhou Institute of Geochemistry, Chinese Academy of Science (GIGCAS 135 project 135TP201601). This is contribution No. IS-2712 from GIGCAS.

Appendix A. Supplementary data

Supplementary data to this article can be found online at https://doi.org/10.1016/j.lithos.2019.05.035.

References

Castillo, P.R., Janney, P.E., Solidum, R.U., 1999. Petrology and geochemistry of Camiguin Island, southern Philippines: insights to the source of adakites and other lavas in a complex arc setting. Contrib. Mineral. Petrol. 134, 33–51.

Castro, A., Gerya, T., García-Casco, A., Fernández, C., Díaz-Alvarado, J., Moreno-Ventas, I., Löw, I., 2010. Melting relations of MORB-sediment mélanges in underplated mantle wedge plumes. Implications for the origin of cordilleran-type batholiths. J. Petrol. 51, 1267–1295.

Castro, A., Vogt, K., Gerya, T., 2013. Generation of new continental crust by sublithospheric silicic-magma relamination in arcs: a test of Taylor's andesite model. Gondw. Res. 23, 1554–1566.

Chen, B., Arakawa, Y., 2005. Elemental and Nd–Sr isotopic geochemistry of granitoids from the West Junggar foldbelt (NWChina), with implications for Phanerozoic continental growth. Geochim. Cosmochim. Acta 69, 1307–1320.

Chen, J., Xu, J., Wang, B., Kang, Z., Li, J., 2010. Origin of Cenozoic alkaline potassic volcanic rocks at KonglongXiang, Lhasa terrane, Tibetan Plateau: Products of partial melting of a mafic lower-crustal source? Chem. Geol. 273, 286–299.

Chen, J., Zhao, W., Xu, J., Wang, B., Kang, Z., 2012. Geochemistry of Miocene trachytes in Bugasi, Lhasa block, Tibetan Plateau: Mixing products between mantle- and crust-derived melts? Gondw. Res. 21 (1), 112–122.

Chen, L., Zhao, Z., Zheng, Y., 2014. Origin of andesitic rocks: Geochemical constraints from Mesozoic volcanics in the Luzong basin, South China. Lithos 220–239.
Chen, Y., Li, W., Yuan, X., Badal, J., Teng, J., 2015. Tearing of the Indian lithospheric slab beneath southern Tibet revealed by SKS-wave splitting measurements. Earth Planet. Sci. Lett. 413, 13–24.
Chu, M.F., Chung, S.L., Song, B., Liu, D.Y., O'Reilly, S.Y., Pearson, N.J., Ji, J.Q., Wen, D.J., 2006. Zircon U-Pb and Hf isotope constraints on the Mesozoic tectonics and crustal evolution of southern Tibet. Geology 34, 745–748.
Chung, S.L., Liu, D.Y., Ji, J.Q., Chu, M.F., Lee, H.Y., Wen, D.J., Lo, C.H., Lee, T.Y., Qian, Q., Zhang, Q., 2003. Adakites from continental collision zones: melting of thickened lower crust beneath southern Tibet. Geology 31, 1021–1024.
Chung, S., Chu, M., Zhang, Y., Xie, Y., Lo, C., Lee, T., Lan, C., Li, X., Zhang, Q., Wang, Y., 2005. Tibetan tectonic evolution inferred from spatial and temporal variations in post-collisional magmatism. Earth-Sci. Rev. 68, 173–196.
Collins, W.J., Richards, S.W., 2008. Geodynamic significance of S-type granites in circum-Pacific orogens. Geology 36, 559–562.
Conticelli, S., Guarnieri, L., Farinelli, A., Mattei, M., Avanzinelli, R., Bianchini, G., Boari, E., Tommasini, S., Tiepolo, M., Prelević, D., Venturelli, G., 2009. Trace elements and Sr–Nd–Pb isotopes of K-rich, shoshonitic, and calc-alkaline magmatism of the Western Mediterranean Region: Genesis of ultrapotassic to calc-alkaline magmatic associations in a post-collisional geodynamic setting. Lithos 107, 68–92.
Dai, F., Zhao, Z., Zheng, Y., 2017. Partial melting of the orogenic lower crust: Geochemical insights from post-collisional alkaline volcanics in the Dabie orogen. Chem. Geol. 25–43.
Davidson, J.P., Turner, S., Handley, H., Macpherson, C.G., Dosseto, A., 2007. Amphibole "sponge" in arc crust? Geology 35 (9), 787–790.
DeCelles, P., Robinson, D., Zandt, G., 2002. Implications of shortening in the Himalayan fold-thrust belt for uplift of the Tibetan Plateau. Tectonics 21, 1–25.
DeCelles, P., Kapp, P., Quade, J., Gehrels, G., 2011. The Oligocene-Miocene Kailas Basin, southwestern Tibet: Record of post-collisional upper plate extension in the Indus-Yarlung suture zone. Geol. Soc. Am. Bull. 123, 1337–1362.
Ding, L., Kapp, P., Zhong, D., Deng, W., 2003. Cenozoic volcanism in Tibet: evidence for a transition from oceanic to continental subduction. J. Petrol. 44, 1833–1865.
Ernst, W.G., 2010. Subduction-zone metamorphism, calc-alkaline magmatism, and convergent-margin crustal evolution. Gondw. Res. 18 (1), 8–16.
Gao, Li-E., Zeng, L.-S., Asimow, P.D., 2017. Contrasting geochemical signatures of fluid-absent versus fluid-fluxed melting of muscovite in metasedimentary sources: the Himalayan leucogranites. Geology 45 (1), 39–42.
Gao, P., Zheng, Y., Chen, Y., Zhao, Z., Xia, X., 2018. Relict zircon U-Pb age and O isotope evidence for reworking of Neoproterozoic crustal rocks in the origin of Triassic S-type granites in South China. Lithos 261–277.
Guo, Z.F., Wilson, M., Liu, J.Q., Mao, Q., 2006. Postcollisional, potassic and ultrapotassic magmatism of the northern Tibetan Plateau: constraints on characteristics of the mantle source, geodynamic setting and uplift mechanisms. J. Petrol. 47, 1177–1220.
Guo, Z.F., Wilson, M., Zhang, M., Cheng, Z., Zhang, L., 2015. Post-collisional ultrapotassic mafic magmatism in South Tibet: Products of partial melting of pyroxenite in the mantle wedge induced by roll-back and delamination of the subducted Indian continental lithosphere slab. J. Petrol. 56, 1365–1406.
Hao, L.-L., Wang, Q., Wyman, D.A., Ou, Q., Dan, W., Jiang, Z.-Q., Wu, F.-Y., Yang, J.-H., Long, X.-P., Li, J., 2016a. Underplating of basaltic magmas and crustal growth in a continental arc: evidence from late Mesozoic intermediate-felsic intrusive rocks in southern Qiangtang, Central Tibet. Lithos 245, 223–242.
Hao, L.-L., Wang, Q., Wyman, D.A., Ou, Q., Dan, W., Jiang, Z.-Q., Yang, J.-H., Li, J., Long, X.-P., 2016b. Andesitic crustal growth via mélange partial melting: evidence from early cretaceous arc dioritic/andesitic rocks in southern Qiangtang, Central Tibet. Geochem. Geophys. Geosyst. 17. https://doi.org/10.1002/2016GC006248.
Hao, L.-L., Wang, Q., Wyman, D., Qi, Y., Ma, L., Huang, F., Zhang, L., Xia, X., Ou, Q., 2018. First identification of mafic igneous enclaves in Miocene lavas of southern Tibet with implications for Indian continental subduction. Geophys. Res. Lett. 45, 8205–8213.
Hao, L.-L., Wang, Q., Wyman, D., Ma, L., Wang, J., Xia, X., Ou, Q., 2019. First identification of postcollisional A-type magmatism in the Himalayan-Tibetan orogen. Geology 47, 187–190.
Hawkesworth, C.J., Cawood, P.A., Dhuime, B., 2016. Tectonics and crustal evolution. GSA Today 26 (9), 4–11.
Hou, Z.Q., Gao, Y.F., Qu, X.M., Rui, Z.Y., Mo, X.X., 2004. Origin of adakitic intrusives generated during mid-Miocene east-west extension in southern Tibet. Earth Planet. Sci. Lett. 220, 139–155.
Hou, Z.Q., Zheng, Y.C., Zeng, L.S., Gao, L.E., Huang, K.X., Li, W., Li, Q.Y., Fu, Q., Liang, W., Sun, Q.Z., 2012. Eocene-Oligocene granitoids in southern Tibet: constraints on crustal anatexis and tectonic evolution of the Himalayan orogen. Earth Planet. Sci. Lett. 349, 38–52.
Hu, X., Garzanti, E., Moore, T., Raffi, I., 2015. Direct stratigraphic dating of India-Asia collision onset at the Selandian (middle Paleocene, 59±1 Ma). Geology 43 (10), 859–862.
Jahn, B.M., 2004. The Central Asian Orogenic Belt and growth of the continental crust in the Phanerozoic. Geol. Soc. Lond. Spec. Publ. 226, 73–100.
Ji, W.Q., Wu, F.Y., Chung, S.L., Li, J.X., Liu, C.Z., 2009. Zircon U-Pb geochronology and Hf isotopic constraints on petrogenesis of the Gangdese batholith, southern Tibet. Chem. Geol. 262, 229–245.
Ji, W.Q., Wu, F.Y., Chung, S.L., Wang, X.C., Liu, C.Z., Li, Q.L., Liu, Z.-C., Liu, X.-C., Wang, J.-G., 2016. Eocene Neo-Tethyan slab breakoff constrained by 45 Ma oceanic island basalt-type magmatism in southern Tibet. Geology 44 (4), 283–286.
Jiang, Z.Q., Wang, Q., Wyman, D.A., Li, Z.X., Yang, J.H., Shi, X.B., Ma, L., Tang, G.-J., Gou, G.N., Jia, X.H., Guo, H.F., 2014. Transition from oceanic to continental lithosphere subduction in southern Tibet: evidence from the late Cretaceous-early Oligocene (~91-30 Ma) intrusive rocks in the Chanang-Zedong area, southern Gangdese. Lithos 196-197, 213–231.
Kelemen, P.B., 1995. Genesis of high Mg# andesites and the continental crust. Contrib. Mineral. Petrol. 120, 1–19.
Kind, R., Ni, J., Zhao, W., Wu, J., Yuan, X., Zhao, L., Sandvol, E., Reese, C., Nabelek, J., Hearn, T., 1996. Evidence from earthquake data for partially molten crustal layer in Southern Tibet. Science 274, 1692–1694.
Leake, B., Woolley, A., Arps, C., Birch, W., Gilbert, M., Grice, J., Hawthorn, F., Kato, A., Kisch, H., Krivovichev, V., 1997. Nomenclature of amphiboles: report of the subcommittee on amphiboles of the Int. Mineral. Assoc., Commission on New Minerals and Mineral Names. Am. Mineral. 82, 1019–1037.
Liu, C.Z., Wu, F.Y., Chung, S.L., Zhao, Z.D., 2011. Fragments of hot and metasomatized mantle lithosphere in Middle Miocene ultrapotassic lavas, southern Tibet. Geology 39 (10), 923–926.
Liu, D., Zhao, Z., Zhu, D., Niu, Y., Depaolo, D.J., Harrison, T.M., Mo, X., Dong, G., Zhou, S., Sun, C., Zhang, Z., Liu, J., 2014. Postcollisional potassic and ultrapotassic rocks in southern Tibet: Mantle and crustal origins in response to India-Asia collision and convergence. Geochim. Cosmochim. Acta 143, 207–231.
Liu, D., Zhao, Z., Depaolo, D.J., Zhu, D., Meng, F., Shi, Q., Wang, Q., 2017. Potassic volcanic rocks and adakitic intrusions in southern Tibet: Insights into mantle-crust interaction and mass transfer from Indian plate. Lithos 48–64.
Ma, L., Wang, Q., Wyman, D.A., Jiang, Z.Q., Yang, J.H., Li, Q.L., Gou, G.N., Guo, H.F., 2013a. Late cretaceous crustal growth in the Gangdese area, southern Tibet: petrological and Sr-Nd-Hf-O isotopic evidence from Zhengga diorite-gabbro. Chem. Geol. 349, 54–70.
Ma, L., Wang, Q., Wyman, D.A., Li, Z.X., Jiang, Z.Q., Yang, J.H., Gou, G.N., Guo, H.F., 2013b. Late cretaceous (100-89 Ma) magnesian charnockites with adakitic affinities in the Milin area, eastern Gangdese: partial melting of subducted oceanic crust and implications for crustal growth in southern Tibet. Lithos 175, 315–332.
Macpherson, C.G., Dreher, S.T., Thirlwall, M.F., 2006. Adakites without slab melting: high pressure differentiation of island arc magma, Mindanao, the Philippines. Earth Planet. Sci. Lett. 243, 581–593.
Miller, C., Schuster, R., Klotzli, U., Frank, W., Purtscheller, F., 1999. Post-collisional potassic and ultrapotassic magmatism in SW Tibet: Geochemical and Sr-Nd-Pb-O isotopic constraints for mantle source characteristics and petrogenesis. J. Petrol. 40 (9), 1399–1424.
Mo, X.X., Niu, Y.L., Dong, G.C., Zhao, Z.D., Hou, Z.Q., Zhou, S., Ke, S., 2008. Contribution of syncollisional felsicmagmatismto continental crust growth: a case study of the Paleogene Linzizong volcanic succession in southern Tibet. Chem. Geol. 250, 49–67.
Müntener, O., Kelemen, P.B., Grove, T.L., 2001. The role of H2O during crystallization of primitive arc magmas under uppermost mantle conditions and genesis of igneous pyroxenites: An experimental study. Contrib. Mineral. Petrol. 141 (6), 643–658.
Müntener, O., Ulmer, P., 2006. Experimentally derived high-pressure cumulates from hydrous arc magmas and consequences for the seismic velocity structure of lower arc crust. Geophys. Res. Lett. 33 (21). https://doi.org/10.1029/2006GL027629.
Müntener, O., Ulmer, P., 2018. Arc crust formation and differentiation constrained by experimental petrology. Am. J. Sci. 318 (1), 64–89.
Nabělek, J., Hetenyi, G., Vergne, J., Sapkota, S.N., Kafle, B., Jiang, M., Su, H., Chen, J., Huang, B., 2009. Underplating in the Himalaya-Tibet collision zone revealed by the hi-CLIMB experiment. Science 325 (5946), 1371–1374.
Nomade, S., Renne, P.R., Mo, X., Zhao, Z., Zhou, S., 2004. Miocene volcanism in the Lhasa block, Tibet: Spatial trends and geodynamic implications. Earth Planet. Sci. Lett. 221 (1–4), 227–243.
Ou, Q., Wang, Q., Wyman, D.A., Zhang, C., Hao, L.-L., Dan, W., Jiang, Z.Q., Wu, F-Y., Yang, J-H., Zhang, H-X., Xia, X-P., Ma, L., Long, X-P., Li, J., 2018. Postcollisional delamination and partial melting of enriched lithospheric mantle: evidence from Oligocene (ca. 30 Ma) potassium-rich lavas in the Gemuchaka area of the central Qiangtang Block, Tibet. Geol. Soc. Am. Bull., doi.org/https://doi.org/10.1130/B31911.1.
Pang, K.N., Chung, S.-L., Zarrinkoub, M.H., Lin, Y.-C., Lee, H.-Y., Lo, C.-H., Khatib, M.M., 2013. Iranian ultrapotassic volcanism at ~11 Ma signifies the initiation of post-collisional magmatism in the Arabia–Eurasia collision zone. Terra Nova 25, 405–413.
Rudnick, R.L., 1995. Making continental crust. Nature 378, 571–577.
Sengör, A.M.C., Natal'In, B.A., Burtman, V.S., 1993. Evolution of the Altaid tectonic collage and Palaeozoic crustal growth in Eurasia. Nature 364, 299–307.
Sun, S., McDonough, W.F., 1989. Chemical and isotopic systematics of oceanic basalts: Implications for mantle composition and processes. In: Saunders, A.D., Norry, M.J. (Eds.), Magmatism in the Ocean Basins. Geological Society, London, Special Publications. vol. 42, pp. 313–345.
Sun, X., Lu, Y.J., McCuaig, T.C., Zheng, Y.-Y., Chang, H.F., Guo, F., Xu, L.-J., 2018. Miocene ultrapotassic, high-Mg dioritic, and adakite-like rocks from Zhunuo in Southern Tibet: implications for mantle metasomatism and porphyry copper mineralization in collisional Orogens. J. Petrol. 59 (3), 341–386.
Tang, M., Erdman, M., Eldridge, G., Lee, C.T.A., 2018. The redox "filter" beneath magmatic orogens and the formation of continental crust. Sci. Adv. 4, eaar4444.
Taylor, S.R., McLennan, S.M., 1985. The Continental Crust: Its Composition and Evolution. Blackwell Scientific Publications, Oxford (312 p).
Turner, S., Arnaud, N., Liu, J., Rogers, N., Hawkesworth, C., Harris, N., Kelley, S., Calsteren, P., Deng, W., 1996. Post-collision, shoshonitic volcanism on the Tibetan Plateau: Implications for convective thinning of the lithosphere and the source of Ocean Island basalts. J. Petrol. 37 (1), 45–71.
Ulmer, P., Kaegi, R., Müntener, O., 2018. Experimentally derived intermediate to silica-rich arc magmas by fractional and equilibrium crystallization at 1.0 GPa: An evaluation of phase relationships, compositions, liquid lines of descent and oxygen fugacity. J. Petrol. 59 (1), 11–58.
Wang, R., Collins, W.J., Weinberg, R.F., Li, J., Li, Q., He, W., Richards, J., Hou, Z., Zhou, L., Stern, R.A., 2016. Xenoliths in ultrapotassic volcanic rocks in the Lhasa block: direct evidence for crust-mantle mixing and metamorphism in the deep crust. Contrib. Mineral. Petrol. 171 (7), 1–19.

Wang, R., Weinberg, R.F., Collins, W.J., Richards, J.P., Zhu, D., 2018. Origin of postcollisional magmas and formation of porphyry Cu deposits in southern Tibet. Earth-Sci. Rev. 122–143.
Williams, H.M., Turner, S.P., Pearce, J.A., Kelley, S.P., Harris, N.B.W., 2004. Nature of the source regions for postcollisional, potassic magmatism in southern and northern Tibet from geochemical variations and inverse trace element modelling. J. Petrol. 45, 555–607.
Wood, B.J., Blundy, J.D., 1997. A predictive model for rare earth element partitioning between clinopyroxene and anhydrous silicatemelt. Contrib. Mineral. Petrol. 129 (2–3), 166–181.
Wu, F.Y., Yang, Y.H., Xie, L.W., Yang, J.H., Xu, P., 2006. Hf isotopic compositions of the standard zircons and baddeleyites used in U-Pb geochronology. Chem. Geol. 234, 105–126.
Wu, F., Liu, Z., Liu, X., Ji, W., 2015. Himalayan leucogranite: Petrogenesis and implications to orogenesis and plateau uplift. Acta Petrol. Sin. 31, 1–36.
Yang, J.H., Chung, S.L., Wilde, S.A., Wu, F.Y., Chu, M.F., Lo, C.H., Fan, H.R., 2005. Petrogenesis of post-orogenic syenites in the Sulu Orogenic Belt, East China: geochronological, geochemical and Nd-Sr isotopic evidence. Chem. Geol. 214, 99–125.
Yang, Z.M., Lu, Y.J., Hou, Z.Q., Chang, Z.S., 2015. High-Mg diorite from qulong in southern Tibet: implications for the genesis of adakite-like intrusions and associated porphyry Cu deposits in collisional orogens. J. Petrol. 56, 227–254.
Yin, A., Harrison, T.M., 2000. Geologic evolution of the Himalayan-Tibetan orogen. Annu. Rev. Earth Planet. Sci. 28, 211–280.
Zeng, L.S., Gao, L.E., Xie, K.J., Jing, L.Z., 2011. Mid-Eocene high Sr/Y granites in the northern Himalayan gneiss domes: melting thickened lower continental crust. Earth Planet. Sci. Lett. 303, 251–266.
Zhang, H.F., Harris, N., Parrish, R., Kelley, S., Zhang, L., Rogers, N., Argles, T., King, J., 2004. Causes and consequences of protractedmelting of themid-crust exposed in the north Himalayan antiform. Earth Planet. Sci. Lett. 228, 195–212.
Zhang, Z.M., Zhao, G.C., Santosh, M., Wang, J.L., Dong, X., Shen, K., 2010. Late cretaceous charnockite with adakitic affinities from the Gangdese batholith, southeastern Tibet: evidence for Neo-Tethyan mid-ocean ridge subduction? Gondw. Res. 17, 615–631.
Zhang, L.Y., Ducea, M.N., Ding, L., Pullen, A., Kapp, P., Hoffman, D., 2014. Southern Tibetan Oligocene-Miocene adakites: a record of Indian slab tearing. Lithos 210-211, 209–223.
Zhang, Z., Dong, X., Xiang, H., Ding, H., He, Z., Liou, J.G., 2015. Reworking of the Gangdese magmatic arc, southeastern Tibet: post-collisional metamorphism and anatexis. J. Metam. Geol. 33 (1), 1–21.
Zhang, L.H., Guo, Z.F., Zhang, M.L., Cheng, Z.H., Sun, Y.T., 2017. Post-collisional potassic magmatism in the eastern Lhasa terrane, South Tibet: Products of partial melting of mélanges in a continental subduction channel. Gondw. Res. 41, 9–28.
Zhao, Z.-F., Zheng, Y.-F., Wei, C.-S., Wu, Y.-B., 2004. Zircon isotope evidence for recycling of subducted continental crust in post-collisional granitoids from the Dabie terrane in China. Geophys. Res. Lett. 31, L22602.
Zhao, Z., Zheng, Y., Wei, C., Wu, Y., 2007. Post-collisional granitoids from the Dabie orogen in China: Zircon U-Pb age, element and O isotope evidence for recycling of subducted continental crust. Lithos 93 (3), 248–272.
Zhao, Z.D., Mo, X., Dilek, Y., Niu, Y., DePaolo, D., Robinson, P., Zhu, D., Sun, C., Dong, G., Zhou, S., Luo, Z., Hou, Z., 2009. Geochemical and Sr-Nd-Pb-O isotopic compositions of the postcollisional ultrapotassic magmatism in SW Tibet: Petrogenesis and implications for India intra-continental subduction beneath southern Tibet. Lithos 113, 190–212.
Zhao, Z., Zheng, Y., Wei, C., Wu, F., 2011. Origin of postcollisional magmatic rocks in the Dabie orogen: implications for crust-mantle interaction and crustal architecture. Lithos 126 (1), 99–114.
Zhao, Z.-F., Zheng, Y.-F., Zhang, J., Dai, L.-Q., Li, Q., Liu, X., 2012. Syn-exhumation magmatism during continental collision: evidence from alkaline intrusives of Triassic age in the Sulu orogen. Chem. Geol. 328, 70–88.
Zhao, Z., Liu, Z., Chen, Q., 2017. Melting of subducted continental crust: Geochemical evidence from Mesozoic granitoids in the Dabie-Sulu orogenic belt, east-Central China. J. Asian Earth Sci. 260–277.
Zheng, Y., 2012. Metamorphic chemical geodynamics in continental subduction zones. Chem. Geol. 5–48.
Zheng, Y., Wu, F., 2018. The timing of continental collision between Indian and Asia. Sci. Bull. 63 (24), 1649–1654.
Zheng, Y., Zhang, S., Zhao, Z., Wu, Y., Li, X., Li, Z., Wu, F., 2007. Contrasting zircon Hf and O isotopes in the two episodes of Neoproterozoic granitoids in South China: implications for growth and reworking of continental crust. Lithos 96 (1), 127–150.
Zheng, Y., Wu, R., Wu, Y., Zhang, S., Yuan, H., Wu, F., 2008. Rift melting of juvenile arc-derived crust: Geochemical evidence from Neoproterozoic volcanic and granitic rocks in the Jiangnan Orogen, South China. Precambrian Res. 163 (3), 351–383.
Zheng, Y.F., Xia, Q.X., Chen, R.X., Gao, X.Y., 2011. Partial melting, fluid supercriticality and element mobility in ultrahigh-pressure metamorphic rocks during continental collision. Earth-Sci. Rev. 107, 342–374.
Zheng, Y., Chen, Y., Dai, L., Zhao, Z., 2015. Developing plate tectonics theory from oceanic subduction zones to collisional orogens. Sci. China-Earth Sci. 58 (7), 1045–1069.
Zhou, X., Zheng, J., Xiong, Q., Yang, J., Wu, Y., Zhao, J., Griffin, W., Dai, H., 2017. Early Mesozoic deep-crust reworking beneath the Central Lhasa terrane (South Tibet): evidence from intermediate gneiss xenoliths in granites. Lithos 225–239.
Zhu, D.C., Mo, X.X., Niu, Y.L., Zhao, Z.D., Wang, L.Q., Liu, Y.S., Wu, F.Y., 2009. Geochemical investigation of early cretaceous igneous rocks along an east-west traverse throughout the Central Lhasa Terrane, Tibet. Chem. Geol. 268, 298–312.
Zhu, D.C., Zhao, Z.D., Niu, Y.L., Mo, X.X., Chung, S.L., Hou, Z.Q., Wang, L.Q., Wu, F.Y., 2011. The Lhasa Terrane: record of a microcontinent and its histories of drift and growth. Earth Planet. Sci. Lett. 301, 241–255.
Zhu, D.C., Zhao, Z.D., Niu, Y.L., Dilek, Y., Hou, Z.Q., Mo, X.X., 2013. The origin and pre-Cenozoic evolution of the Tibetan Plateau. Gondw. Res. 23, 1429–1454.
Zhu, D., Wang, Q., Zhao, Z., Chung, S., Cawood, P.A., Niu, Y., Liu, S., Wu, F., Mo, X., 2015. Magmatic record of India-Asia collision. Sci. Rep. 5, 14289.
Zhu, D., Wang, Q., Chung, S., Cawood, P.A., Zhao, Z., 2018. Gangdese magmatism in southern Tibet and India-Asia convergence since 120 Ma. Geol. Soc. Lond. Spec. Publ. 483.